

# A Cell-Based Molecular Transport Simulator for Pharmacokinetic Prediction and Cheminformatic Exploration

Xinyuan Zhang,<sup>†</sup> Kerby Shedden,<sup>‡,§</sup> and Gus R. Rosania<sup>\*,†,§</sup>

Michigan Alliance for Cheminformatic Exploration, University of Michigan,  
Department of Pharmaceutical Science, University of Michigan College of Pharmacy, and  
Department of Statistics, University of Michigan, Ann Arbor, Michigan 48109

Received April 18, 2006; Revised Manuscript Received August 30, 2006; Accepted September 22, 2006

**Abstract:** In the body, cell monolayers serve as permeability barriers, determining transport of molecules from one organ or tissue compartment to another. After oral drug administration, for example, transport across the epithelial cell monolayer lining the lumen of the intestine determines the fraction of drug in the gut that is absorbed by the body. By modeling passive transcellular transport properties in the presence of an apical to basolateral concentration gradient, we demonstrate how a computational, cell-based molecular transport simulator can be used to define a physicochemical property space occupied by molecules with desirable permeability and intracellular retention characteristics. Considering extracellular domains of cell surface receptors located on the opposite side of a cell monolayer as a drug's desired site of action, simulation of transcellular transport can be used to define the physicochemical properties of molecules with maximal transcellular permeability but minimal intracellular retention. Arguably, these molecules would possess very desirable features: least likely to exhibit nonspecific toxicity, metabolism, and side effects associated with high (undesirable) intracellular accumulation; and most likely to exhibit favorable bioavailability and efficacy associated with maximal rates of transport across cells and minimal intracellular retention, resulting in (desirable) accumulation at the extracellular site of action. Simulated permeability values showed good correlations with PAMPA, Caco-2, and intestinal permeability measurements, without "training" the model and without resorting to statistical regression techniques to "fit" the data. Therefore, cell-based molecular transport simulators could be useful in silico screening tools for chemical genomics and drug discovery.

**Keywords:** Metoprolol; permeability; chemical space; computer aided drug design; virtual screening; chemical genomics; cellular pharmacokinetics; cheminformatics; drug transport; PAMPA; Biopharmaceutics Classification System

## Introduction

Drug uptake and transport across cell monolayers is an important determinant of in vivo bioavailability, biodistribution, and activity.<sup>1</sup> However, enzymes of low selectivity

metabolize drugs inside cells.<sup>2,3</sup> High permeability—high solubility drugs administered at high concentrations diffuse across cells fast enough—saturating transporters and enzymes—that only an insignificant fraction is diverted.<sup>4,5</sup> However, high intracellular drug concentrations can also be toxic. For example, unwanted accumulation of small molecules in mitochondria can interfere with mitochondrial function, inducing apoptosis.<sup>6,7</sup> Similarly, unintentional accumulation

\* To whom correspondence should be addressed. Mailing address: Department of Pharmaceutical Sciences, University of Michigan College of Pharmacy, 428 Church Street, Ann Arbor, Michigan 48109. E-mail: grosania@umich.edu. Phone: 734-763-1032. Fax: 734-615-6162.

<sup>†</sup> Department of Pharmaceutical Science, University of Michigan College of Pharmacy.

<sup>‡</sup> Department of Statistics, University of Michigan.

<sup>§</sup> Michigan Alliance for Cheminformatic Exploration, University of Michigan.

(1) Artursson, P.; Karlsson, J. *Biochem. Biophys. Res. Commun.* **1991**, 175 (3), 880–885.

(2) Wachter, V. J.; Salphati, L.; Benet, L. Z. *Adv. Drug Delivery Rev.* **2001**, 46 (1–3), 89–102.

(3) Graham-Lorence, S.; Peterson, J. A. *FASEB J.* **1996**, 10 (2), 206–214.

of molecules in other organelles can induce phenotypic effects unrelated to a drug's primary mechanism of action—manifesting as nonspecific toxicity.<sup>8</sup> Nevertheless, many drugs are agonists or antagonists of cell surface receptors.<sup>9</sup> Since receptor ligand binding domains are extracellular, intracellular drug accumulation is not essential for bioactivity.<sup>10</sup> Thus, molecules designed to reach and accumulate at a desired extracellular site of action should combine high transcellular permeability with minimal intracellular accumulation. These desirable biopharmaceutical properties can lead, in turn, to more potent, bioavailable, stable, and nontoxic drug candidates.

Poor pharmacokinetics and toxicity are important causes of failure in the later, clinical stages of drug development.<sup>4,11,12</sup> Therefore, ADMET (absorption, distribution metabolism, elimination, and toxicity) profiling is desirable as early as possible, before drug candidates are tested in patients. High throughput in silico ADMET models are one way to predict favored pharmacokinetics and toxicity profiles, early in the design of new drugs.<sup>12</sup> Mapping chemical spaces occupied by molecules possessing a desirable therapeutic activity and favored ADMET properties can be used to guide the design, synthesis, and selection of series of lead compounds.<sup>13–15</sup> Along these lines, we sought to develop a fast, flexible, and scalable computational tool for predicting epithelial transcellular passive permeability and intracellular accumulation, which are important determinants of oral absorption prediction and toxicity prediction, respectively.<sup>16–18</sup>

Drug solubility and intestinal permeability are the two key criteria for the FDA's Biopharmaceutics Classification System (BCS).<sup>19</sup> At early stages of drug development mathematical models built on the basis of data derived from in vitro experiments such as PAMPA (parallel artificial

membrane permeation assay) and Caco-2 assay are widely used to predict human intestinal permeability. Most existing mathematical models to predict intestinal permeability are based on statistical regression methods that correlate PAMPA, Caco-2, or rat or human intestinal permeability measurements to 2D and/or 3D molecular descriptors.<sup>20–22</sup> However, the predictive power of these statistical models is inherently dependent on the quality of training data set, as well as the variability and reproducibility of the experimental assay. Furthermore, because of the statistical nature of the regression relationship, large amounts of data are needed to generate good models covering large realms of chemical space. To complement statistical regression methods, we decided to pursue a mechanism-based, mathematical modeling strategy to predict transcellular passive permeability, while also predicting the intracellular concentration of drug and its accumulation in organelles. In addition, on the basis of permeability and intracellular concentration of a reference “lead” compound, we also sought a nonstatistical method that could map cell-permeant/impermeant and cell-toxic/nontoxic chemical spaces relative to that compound, to help guide drug lead development efforts of pharmaceutical scientists and medicinal chemists.

Here, we present a mechanism-based modeling strategy that can predict intestinal transcellular passive permeability, as well as drug accumulation within cells. Mathematically, the model describes transcellular transport of small molecules based on a physical, compartmental model of a cell, coupling sets of differential equations describing the physics of passive diffusion of small molecules across membranes delimiting the different compartments.<sup>23</sup> Without incorporating enzymatic mechanisms or specific binding interactions, the current version of the model can predict the behavior of nonzwitterionic, monocharged small molecules possessing one ionizable functional group in the physiological pH range. Nevertheless, the behavior of more complex molecules and mechanisms—such as carrier mediated transport, metabolic processes, or multiple ionizable groups—can be incorporated one by one in subsequent versions of the model, to predict the transport of low permeability, natural productlike molecules, and to mimic more complex, physiological conditions.

## Methods

Starting with a cell-based, molecular mass transport model developed to study the accumulation of lipophilic cations in

- (4) Cao, X.; Yu, L. X.; Barbaciru, C.; Landowski, C. P.; Shin, H. C.; Gibbs, S.; Miller, H. A.; Amidon, G. L.; Sun, D. *Mol. Pharm.* **2005**, *2* (4), 329–40.
- (5) Varma, M. V.; Sateesh, K.; Panchagnula, R. *Mol. Pharm.* **2005**, *2* (1), 12–21.
- (6) Fantin, V. R.; Leder, P. *Cancer Res.* **2004**, *64* (1), 329–336.
- (7) Modica-Napolitano, J. S.; Aprille, J. R. *Adv. Drug Delivery Rev.* **2001**, *49* (1–2), 63–70.
- (8) Wallace, K. B. *Pharmacol. Toxicol.* **2003**, *93* (3), 105–115.
- (9) Freddolino, P. L.; Kalani, M. Y. S.; Vaidehi, N.; Floriano, W. B.; Hall, S. E.; Trabanino, R. J.; Kam, V. W. T.; Goddard, W. A. *Proc. Natl. Acad. Sci. U.S.A.* **2004**, *101* (9), 2736–2741.
- (10) Fitzsimmons, T. J.; Zhao, X. L.; Wank, S. A. *J. Biol. Chem.* **2003**, *278* (16), 14313–14320.
- (11) Kennedy, T. *Drug Discovery Today* **1997**, *2* (10), 436–444.
- (12) Camenisch, G.; Alsenz, J.; van de Waterbeemd, H.; Folkers, G. *Eur. J. Pharm. Sci.* **1998**, *6* (4), 317–324.
- (13) Lloyd, D. G.; Golfis, G.; Knox, A. J.; Fayne, D.; Meegan, M. J.; Oprea, T. I. *Drug Discovery Today* **2006**, *11* (3–4), 149–159.
- (14) Oprea, T. I.; Zamora, I.; Ungell, A. L. *J. Comb. Chem.* **2002**, *4* (4), 258–266.
- (15) Oprea, T. I. *Curr. Opin. Chem. Biol.* **2002**, *6* (3), 384–389.
- (16) Balaz, S.; Lukacova, V. *J. Mol. Graphics Modell.* **2002**, *20* (6), 479–490.
- (17) Balaz, S.; Pirslova, K.; Schultz, T. W.; Hermens, J. *J. Theor. Biol.* **1996**, *178* (1), 7–16.

- (18) Dvorsky, R.; Balaz, S.; Sawchuk, R. J. *J. Theor. Biol.* **1997**, *185* (2), 213–222.
- (19) Amidon, G. L.; Lennernas, H.; Shah, V. P.; Crison, J. R. *Pharm. Res.* **1995**, *12* (3), 413–420.
- (20) Stenberg, P.; Luthman, K.; Artursson, P. *Pharm. Res.* **1999**, *16* (2), 205–212.
- (21) Norinder, U.; Osterberg, T.; Artursson, P. *Pharm. Res.* **1997**, *14* (12), 1786–1791.
- (22) Winiwarter, S.; Bonham, N. M.; Ax, F.; Hallberg, A.; Lennernas, H.; Karlen, A. *J. Med. Chem.* **1998**, *41* (25), 4939–4949.
- (23) Trapp, S.; Horobin, R. W. *Eur. Biophys. J.* **2005**, *34* (7), 959–966.

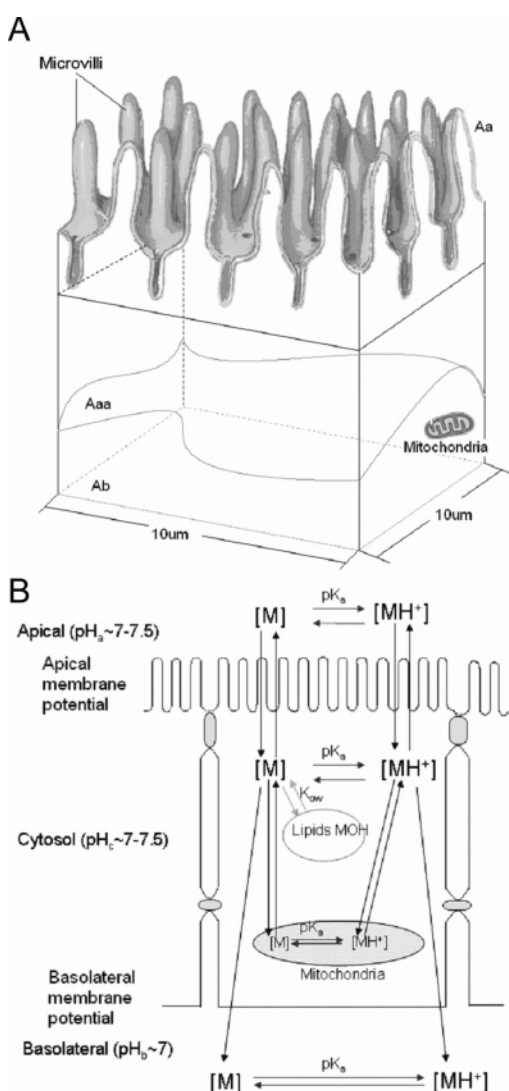


**Figure 1.** Model of an intestinal epithelial cell. (A) Cell morphology. (B) The path of a hydrophobic weak base across an intestinal epithelial cell. The neutral form of the molecule is indicated as [M], and the protonated, cationic form of the molecule is indicated as [MH<sup>+</sup>].

tumor cells,<sup>23</sup> we adapted the Nernst–Planck and Fick equations to simulate transport of molecules across epithelial cell monolayers, in the presence of an apical-to-basolateral, transcellular concentration gradient. For a weakly basic/acid, druglike small molecule, the cellular pharmacokinetic model considers three physicochemical properties as the most important determinants of intracellular accumulation and transport: (1) the logarithm of the lipid/water partition coefficient of the neutral form of the molecule, log  $P_n$ ; (2) the logarithm of the lipid/water partition coefficient of the ionized form of the molecule, log  $P_d$ ; and (3) the negative logarithm of the dissociation constant of the protonated functional group, pK<sub>a</sub>. Drug concentrations in different intracellular compartments are coupled to each other according to the topological organization of the cell (Figure 1A,B). Different organelles have different pHs and transmembrane electrical potentials, so a molecule's charge in

different organelles can vary according to the molecule's pK<sub>a</sub>; and transport properties across the membranes delimiting different compartments can vary depending on the membranes' electrical potential.<sup>24–27</sup> With the model developed herein, the concentration of molecules in different subcellular compartments and the transcellular permeability coefficient ( $P_{eff}$ ) can be calculated for different time intervals after cells are exposed to drug (see Supporting Information).

For modeling drug accumulation in the cytosolic compartment, the mitochondrial compartment, and the basolateral compartment, the total mass change of the molecule with time can be expressed by eqs 1–3:

$$\frac{dm_c}{dt} = A_a J_{a,c} - A_m J_{c,m} - A_b J_{c,b} \quad (1)$$

$$\frac{dm_m}{dt} = A_m J_{c,m} \quad (2)$$

$$\frac{dm_b}{dt} = A_b J_{c,b} \quad (3)$$

where  $J$  is the net flux from the “positive” side to the “negative” side,  $m$  is the total molecular mass,  $t$  is time,  $A$  is membrane surface area, and subscripts c, a, b, and m indicate cytosolic, apical, basolateral, and mitochondrial, respectively. The direction from apical to basolateral compartment was defined from the “positive” side to the “negative” side.

To solve the above equations, the relationships between fluxes and masses must be specified. The bridge between these quantities is the concentration in each compartment. Each side of eqs 1, 2, and 3 is divided by the volumes of each compartment to get eqs 4, 5, and 6:

$$\frac{dC_c}{dt} = \frac{A_a}{V_c} J_{a,c} - \frac{A_m}{V_c} J_{c,m} - \frac{A_b}{V_c} J_{c,b} \quad (4)$$

$$\frac{dC_m}{dt} = \frac{A_m}{V_m} J_{c,m} \quad (5)$$

$$\frac{dC_b}{dt} = \frac{A_b}{V_b} J_{c,b} \quad (6)$$

where  $C_c$ ,  $C_m$ , and  $C_b$  are cytosolic, mitochondrial, and basolateral concentration and  $V_c$ ,  $V_m$ , and  $V_b$  are volumes of cytosolic, mitochondrial, and basolateral compartments, respectively. The passive diffusion flux of neutral molecules across membranes is described by Fick's First Law:

(24) Duvvuri, M.; Gong, Y. P.; Chatterji, D.; Krise, J. P. *J. Biol. Chem.* **2004**, 279 (31), 32367–32372.

(25) Davis, S.; Weiss, M. J.; Wong, J. R.; Lampidis, T. J.; Chen, L. B. *J. Biol. Chem.* **1985**, 260 (25), 3844–3850.

(26) Shedden, K.; Brumer, J.; Chang, Y. T.; Rosania, G. R. *J. Chem. Inf. Comput. Sci.* **2003**, 43 (6), 2068–2080.

(27) Chen, V. Y.; Khersonsky, S. M.; Shedden, K.; Chang, Y. T.; Rosania, G. R. *Mol. Pharm.* **2004**, 1 (6), 414–425.

$$J = P(a_o - a_i) \quad (7)$$

where  $J$  is the molecular flux from the outside to the inside (i) (“negative” side) of the membrane,  $P$  is the permeability of the molecules across cellular membranes, and  $a$  is the activity of the molecules. For electrolytes the driving forces across cellular membrane are not only chemical potential but also electrical potential, which is described by the Nernst–Planck equation. With the assumption of a linear potential gradient across the membrane and a net current flow of zero and with each ion flux at steady state, an analytical solution for the flux of the ion is

$$J = P \frac{N}{e^N - 1} (a_o - a_i e^N) \quad (8)$$

where  $N = zEF/RT$ ,  $z$  is the electric charge,  $F$  is the Faraday constant,  $E$  is the membrane potential,  $R$  is the universal gas constant, and  $T$  is the absolute temperature.<sup>23</sup> If eqs 7 and 8 are combined, the net fluxes across each membrane for both neutral forms and ionic forms can be described by eq 9:

$$J = P_n(a_{o,n} - a_{i,n}) + P_d \frac{N}{e^N - 1} (a_{o,d} - a_{i,d} e^N) \quad (9)$$

where  $P_n$  is the permeability of neutral form across the membrane;  $P_d$  is the permeability of the ionized form across the membrane;  $a_{o,n}$  and  $a_{i,n}$  are the activities of the neutral form outside and inside, respectively; and  $a_{o,d}$  and  $a_{i,d}$  are the activities of the ionized form outside and inside, respectively. So the net fluxes across each membrane are

$$J_{a,c} = P_n(a_{n,a} - a_{n,c}) + P_d \frac{N_a}{e^{N_a} - 1} (a_{d,a} - a_{d,c} e^{N_a}) \quad (10)$$

$$J_{c,m} = P_n(a_{n,c} - a_{n,m}) + P_d \frac{N_m}{e^{N_m} - 1} (a_{d,c} - a_{d,m} e^{N_m}) \quad (11)$$

$$J_{c,b} = P_n(a_{n,c} - a_{n,b}) + P_d \frac{N_b}{e^{N_b} - 1} (a_{d,c} - a_{d,b} e^{N_b}) \quad (12)$$

where  $J_{a,c}$ ,  $J_{c,m}$ , and  $J_{c,b}$  are net flux across apical membrane, mitochondrial membrane, and basolateral membrane, respectively;  $a_{a,n}$ ,  $a_{c,n}$ ,  $a_{m,n}$ , and  $a_{b,n}$  are the neutral molecular form activities in the apical compartment, cytosolic compartment, mitochondrial compartment, and basolateral compartment, respectively;  $a_{a,d}$ ,  $a_{c,d}$ ,  $a_{m,d}$ , and  $a_{b,d}$  are the ionized molecular form activities in the apical compartment, cytosolic compartment, mitochondrial compartment, and basolateral compartment, respectively; and  $N_a$ ,  $N_m$ , and  $N_b$  are the  $N$  values for apical membrane, mitochondrial membrane, and basolateral membrane, respectively. The Henderson–Hasselbalch equation (eq 13) describes the activity ratio of neutral form molecules and ionized form molecules,

$$\log \frac{a_d}{a_n} = i(\text{pH} - \text{p}K_a) \quad (13)$$

where  $a_d$  and  $a_n$  are the ionized molecular form and the neutral molecular form, respectively;  $i$  is 1 for acids and  $-1$

for bases; and  $\text{p}K_a$  is the negative logarithm of the dissociation constant. Therefore,

$$a_d = a_n \times 10^{i(\text{pH} - \text{p}K_a)} \quad (14)$$

The relationship of the activities ( $a_n$  and  $a_d$ ) and the total molecular concentration can be expressed by eqs 15 and 16,<sup>28</sup>

$$f_n = a_n/C_t = \frac{1}{W/\gamma_n + K_n/\gamma_n + W \times 10^{i(\text{pH} - \text{p}K_a)/\gamma_d} + K_d \times 10^{i(\text{pH} - \text{p}K_a)/\gamma_d}} \quad (15)$$

$$f_d = a_d/C_t = f_n \times 10^{i(\text{pH} - \text{p}K_a)} \quad (16)$$

$W$  is the volumetric water fraction,  $\gamma$  is the activity coefficient, and  $K_n$  and  $K_d$  are the sorption coefficients of the neutral and the ionized molecules, respectively.  $K_n$  and  $K_d$  are estimated by eq 17, where  $L$  is the lipid fraction in each compartment and  $K_{ow,n/d} = 10^{\log P_{n,d,lip}}$  ( $\log P_{n,lip}$  and  $\log P_{d,lip}$  calculated with eqs 28–31).

$$K_{n/d} = L \times 1.22 \times K_{ow,n/d} \quad (17)$$

The activity coefficient of all neutral molecules ( $\gamma_n$ ) is related to the ionic strength  $I$  (moles). Using the Setchenov equation, at  $I = 0.3$  mol,  $\gamma_n$  is 1.23. The activity of ions ( $\gamma_d$ ) is calculated with the Davies approximation of the modified Debye–Hückel equation.<sup>23</sup> For monovalent ions at  $I = 0.3$  mol,  $\gamma_d$  is 0.74. For conditions outside the cell, no corrections for the ionic strength are made, and activities are set approximately equal to concentration ( $\gamma = 1$ ).<sup>23</sup> Plug eqs 15 and 16 into eqs 10, 11, and 12 to get eqs 18, 19, and 20.

$$J_{a,c} = P_n(f_{n,a}C_a - f_{n,c}C_c) + P_d \frac{N_a}{e^{N_a} - 1} (f_{d,a}C_a - f_{d,c}C_c e^{N_a}) \quad (18)$$

$$J_{c,m} = P_n(f_{n,c}C_c - f_{n,m}C_m) + P_d \frac{N_m}{e^{N_m} - 1} (f_{d,c}C_c - f_{d,m}C_m e^{N_m}) \quad (19)$$

$$J_{c,b} = P_n(f_{n,c}C_c - f_{n,b}C_b) + P_d \frac{N_b}{e^{N_b} - 1} (f_{d,c}C_c - f_{d,b}C_b e^{N_b}) \quad (20)$$

Plug eqs 18, 19, and 20 into eqs 4, 5, and 6 to get eqs 21, 22, and 23.

$$\frac{dC_c}{dt} = \frac{A_a}{V_c} \left[ P_n(f_{n,a}C_a - f_{n,c}C_c) + P_d \frac{N_a}{e^{N_a} - 1} (f_{d,a}C_a - f_{d,c}C_c e^{N_a}) \right] - \frac{A_c}{V_c} \left[ P_n(f_{n,c}C_c - f_{n,m}C_m) + P_d \frac{N_m}{e^{N_m} - 1} (f_{d,c}C_c - f_{d,m}C_m e^{N_m}) \right] - \frac{A_b}{V_c} \left[ P_n(f_{n,c}C_c - f_{n,b}C_b) + P_d \frac{N_b}{e^{N_b} - 1} (f_{d,c}C_c - f_{d,b}C_b e^{N_b}) \right] \quad (21)$$

(28) Trapp, S. *Environ. Sci. Pollut. Res. Int.* **2004**, *11* (1), 33–39.



$$\frac{dC_m}{dt} = \frac{A_m}{V_m} \left[ P_n(f_{n,c}C_c - f_{n,m}C_m) + P_d \frac{N_m}{e^{N_m} - 1} (f_{d,c}C_c - f_{d,m}C_m e^{N_m}) \right] \quad (22)$$

$$\frac{dC_b}{dt} = \frac{A_b}{V_b} \left[ P_n(f_{n,c}C_c - f_{n,b}C_b) + P_d \frac{N_b}{e^{N_b} - 1} (f_{d,c}C_c - f_{d,b}C_b e^{N_b}) \right] \quad (23)$$

The membrane permeability  $P^{23}$  can be estimated using

$$P = DK/\Delta x \quad (24)$$

$D$  is the diffusion coefficient, which is about  $10^{-14}$  m<sup>2</sup>/s for organic molecules in biomembranes.  $K$  is the partition coefficient and approximates  $K_{ow}$ .  $\Delta x$  is the membrane thickness and is considered about 50 nm for biomembranes. Plugging these estimated numbers into eq 24 and doing a logarithm conversion gives eq 25.

$$\log P = \log K_{ow} - 6.7 \quad (25)$$

Per definition, the transcellular permeability coefficient ( $P_{eff}$ ) is calculated using

$$P_{eff} = \frac{dC_b \times V_b}{dt \times A_{aa} C_a} \quad (26)$$

where  $A_{aa}$  is the cellular monolayer area,  $dC_b$  the total concentration change in basolateral compartment with time  $dt$ , and  $C_a$  the concentration in apical compartment, which is assumed to be constant in this model.

MATLAB was used to solve the system of coupled differential equations (eqs 21, 22, and 23). The concentrations in cytosol ( $C_c$ ), mitochondria ( $C_m$ ), basolateral compartment ( $C_b$ ), and transcellular permeability coefficient ( $P_{eff}$ ) were solved numerically. Cellular parameters describing the intestinal epithelial cell were obtained from the literature. The MATLAB solver, graphics scripts, and model parameters are included as Supporting Information.

Using this model, permeability and intracellular concentration of 36 compounds were calculated (Figures 2, 3). These compounds were selected on the basis of the following criteria: (1) they are monoionized or neutral in the physiological pH environment; (2) their  $\log P_n$ ,  $pK_a$ , and Caco-2 permeability were experimentally measured and published. The octanol/water partition coefficients ( $\log P_n$ ) were obtained from SRC PhysProp Database and other references in the scientific literature,<sup>29–31</sup> and  $pK_a$  values were also experimental data obtained from several published articles.<sup>10,32–40</sup> The partition coefficients of the ionized state

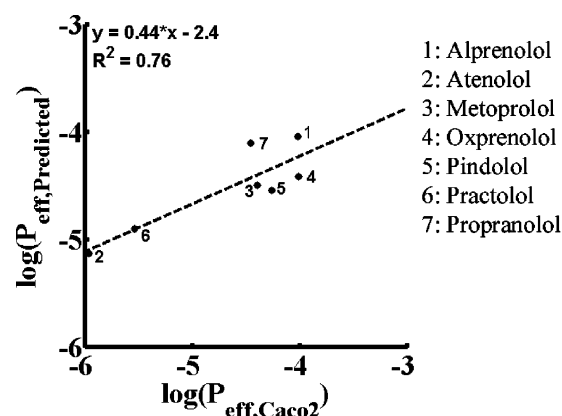


**Figure 2.** Measured Caco-2 permeability and predicted permeability of  $\beta$ -adrenergic receptor blockers are correlated. The x-axis indicates the logarithm values of average measured Caco-2 permeability (cm/s), and the y-axis indicates the logarithm values of predicted permeability (cm/s). The dotted line is the linear regression line. The linear regression equation is  $y = 0.44x - 2.4$  ( $R^2 = 0.76$ ), and the significance  $F$  of regression is 0.011 (confidence level is 95%). Numbers 1 through 7 indicate alprenolol, atenolol, metoprolol, oxprenolol, pindolol, practolol, and propranolol, respectively. The structures, physicochemical properties, average Caco-2 permeability, and predictive permeability are summarized in Table 1.

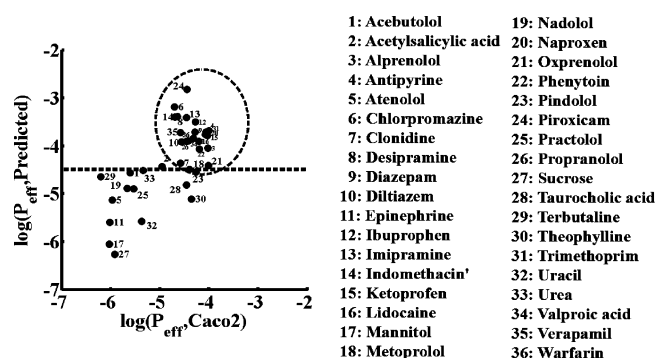


**Figure 3.** Measured Caco-2 permeability and predicted permeability of weakly acidic or basic (nonzwitterionic) drugs with a single ionizable functional group at physiological pH. The x-axis indicates the logarithm values of average measured Caco-2 permeability (cm/s), and the y-axis indicates the logarithm values of predicted permeability (cm/s). Metoprolol (No. 18) was used as a reference drug to define predicted high vs low permeability categories (dashed line). Compounds in the predicted high permeability category exhibit high Caco-2 permeabilities (dashed oval). More detailed information and references relevant to the calculated and average Caco-2 permeability measurements are included in the Supporting Information.

of the molecules ( $\log P_d$ ) were estimated from  $\log P_n$  according to eq 27:<sup>23</sup>

$$\log P_d = \log P_n - 3.7 \quad (27)$$

Equations 28–32 were used to obtain the liposomal partition coefficient for both neutral forms and ionic forms

(29) Interactive PhysProp Database Demo; available from Syracuse Research Corporation (SRC), U.S.A. <http://www.syrres.com/esc/physdemo.htm>.

(30) Xing, L.; Glen, R. C. *J. Chem. Inf. Comput. Sci.* **2002**, *42* (4), 796–805.

(31) Vrakas, D.; Giaginis, C.; Tsantili-Kakoulidou, A. *J. Chromatogr. A* **2006**, *1116* (1–2), 158–164.

of bases and acids.<sup>34</sup> For ampholytes to get the liposomal partitioning, the equation for neutral forms of bases was applied.

for neutral forms of bases:

$$\log P_{n,\text{lip}} = 0.33 \log P_n + 2.2, \quad R^2 = 0.69 \quad (28)$$

for cationic forms of bases:

$$\log P_{d,\text{lip}} = 0.37 \log P_d + 2, \quad R^2 = 0.49 \quad (29)$$

for neutral forms of acids:

$$\log P_{n,\text{lip}} = 0.37 \log P_n + 2.2, \quad R^2 = 0.89 \quad (30)$$

for anionic forms of acids:

$$\log P_{d,\text{lip}} = 0.33 \log P_d + 2.6, \quad R^2 = 0.72 \quad (31)$$

Additional literature references,  $\log P_n$ ,  $\log P_d$ ,  $\text{p}K_a$  values, and calculated permeability and intracellular concentration obtained with our model are included in the Supporting Information.

Linear regression was used to compare predicted permeability values with the Caco-2, PAMPA, and human intestinal permeability adopted from the literature.<sup>1,12,40–47</sup> As noticed, Caco-2 permeability data obtained from different references differ even for the same drug, thus the mean values of Caco-2 permeability obtained from different literature sources were used to compare with the predicted permeability (see Supporting Information).

- (32) Zhou, C.; Jin, Y.; Kenseth, J. R.; Stella, M.; Wehmeyer, K. R.; Heineman, W. R. *J. Pharm. Sci.* **2005**, *94* (3), 576–589.
- (33) Ishihama, Y.; Nakamura, M.; Miwa, T.; Kajima, T.; Asakawa, N. *J. Pharm. Sci.* **2002**, *91* (4), 933–942.
- (34) Balon, K.; Riebesehl, B. U.; Muller, B. W. *Pharm. Res.* **1999**, *16* (6), 882–888.
- (35) Wohnsland, F.; Faller, B. *J. Med. Chem.* **2001**, *44* (6), 923–930.
- (36) McDevitt, D. G. *Eur. Heart J.* **1987**, *8* (Suppl. M), 9–14.
- (37) Avdeef, A.; Artursson, P.; Neuhoff, S.; Lazorova, L.; Grasjo, J.; Tavelin, S. *Eur. J. Pharm. Sci.* **2005**, *24* (4), 333–349.
- (38) Martinez, V.; Maguregui, M. I.; Jimenez, R. M.; Alonso, R. M. *J. Pharm. Biomed. Anal.* **2000**, *23*, (2–3), 459–468.
- (39) Castela-Papin, N.; Cai, S.; Vatie, J.; Souleau, C. H.; Farinotti, R. *Int. J. Pharm.* **1999**, *182* (1), 111–119.
- (40) Palm, K.; Luthman, K.; Ungell, A. L.; Strandlund, G.; Artursson, P. *J. Pharm. Sci.* **1996**, *85* (1), 32–39.
- (41) Yee, S. *Pharm. Res.* **1997**, *14* (6), 763–766.
- (42) Yazdani, M.; Glynn, S. L.; Wright, J. L.; Hawi, A. *Pharm. Res.* **1998**, *15* (9), 1490–1494.
- (43) Gres, M. C.; Julian, B.; Bourrie, M.; Meunier, V.; Roques, C.; Berger, M.; Boulenc, X.; Berger, Y.; Fabre, G. *Pharm. Res.* **1998**, *15* (5), 726–733.
- (44) Irvine, J. D.; Takahashi, L.; Lockhart, K.; Cheong, J.; Tolan, J. W.; Selick, H. E.; Grove, J. R. *J. Pharm. Sci.* **1999**, *88* (1), 28–33.
- (45) Hovgaard, L.; Brondsted, H.; Buur, A.; Bundgaard, H. *Pharm. Res.* **1995**, *12* (3), 387–392.
- (46) Pade, V.; Stavchansky, S. *Pharm. Res.* **1997**, *14* (9), 1210–1215.
- (47) Kasim, N. A.; Whitehouse, M.; Ramachandran, C.; Bermejo, M.; Lennernas, H.; Hussain, A. S.; Junginger, H. E.; Stavchansky, S. A.; Midha, K. K.; Shah, V. P.; Amidon, G. L. *Mol. Pharm.* **2004**, *1* (1), 85–96.

Cell-permeant nontoxic chemical space, cell-permeant toxic chemical space, cell-impermeant chemical space, cell-permeant chemical space, cell-toxic chemical space, and cell-nontoxic chemical space were defined by calculating  $P_{\text{eff}}$ ,  $C_c$ , and  $C_m$  of weakly basic monocationic molecules spanning  $\text{p}K_a$  from 1 to 14,  $\log P_n$  from  $-5$  to  $+5$ , and  $\log P_d$  from  $-5$  to  $+5$ . Each one of these physicochemical parameters was varied independently in 0.1 unit intervals, and combined with the other parameters. To evaluate the robustness of the results obtained with the model, chemical space plots were visually inspected for reproducibility and consistency after changing one parameter at a time while keeping the others unchanged. The changes of  $\log P_n$  and  $\log P_d$  were evaluated under two conditions: (1)  $\log P_n$  and  $\log P_d$  varied independently; and (2)  $\log P_n$  and  $\log P_d$  linked to each other by eqs 27 to 31. Parameter values used in calculation as well as graphing scripts are included in the Supporting Information. More detailed methods and results of testing the model for self-consistency and robustness are described in the Supporting Information.

## Results

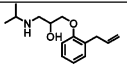
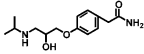
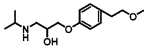
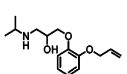
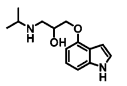
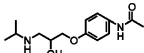
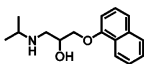
**A Cellular Pharmacokinetic Model of Passive Transcellular Drug Transport.** Transcellular permeability is a key property determining biodistribution of soluble drug molecules from one body compartment to another. For an orally administered drug with high solubility, the transcellular permeability of the cells lining the intestine determines the fraction of drug in the intestine that is absorbed by the body.

In epithelial cells lining the lumen of the intestine (Figure 1A), apical microvilli make the apical surface area<sup>48</sup> much greater than the basolateral surface area.<sup>9</sup> The length of an epithelial cell is approximately 10 to 15  $\mu\text{m}$ .  $A_{\text{aa}}$  is the effective cross-sectional area of each cell, corresponding to the total area of the cell monolayer across which transport occurs, divided by the total number of cells involved in the transcellular transport process. Finally, the total volume of the cell  $V$  constrains its overall geometry in relation to  $A_{\text{a}}$ ,  $A_{\text{b}}$ , and  $A_{\text{aa}}$ . On the basis of these parameters, the apical-to-basolateral permeability of an intestinal epithelial cell can be calculated with eq 26.

Setting cellular parameters to mimic an intestinal epithelial cell, the model captures the mass transport process followed by a weak base or acid (nonzwitterionic molecule), through said cell (Figure 1B). Such molecules exist as equilibrium mixtures of neutral and ionic states, their proportions determined by the pH of the immediate environment. In the case of high solubility–high permeability molecules, passive diffusion is the dominant transcellular transport mechanism,<sup>4,5,46,49</sup> driven by concentration gradients of drugs and ions, and the transmembrane electrical potential. Assuming that mixing of molecules within the intracellular compartments is faster than the rate at which the molecules traverse

- (48) Refsgaard, H. H. F.; Jensen, B. F.; Brockhoff, P. B.; Padkjaer, S. B.; Guldbrandt, M.; Christensen, M. S. *J. Med. Chem.* **2005**, *48* (3), 805–811.

**Table 1.** Structures, Physicochemical Properties, Average Caco-2 Permeabilities, and Predictive Permeabilities of Seven  $\beta$ -Adrenergic Blockers in Figure 2<sup>a</sup>

Name	Structures	pK <sub>a</sub>	logP <sub>n</sub> <sup>29</sup>	logP <sub>n, lip</sub>	Caco-2 P <sub>eff</sub> (10 <sup>-6</sup> cm/s)	Calculated		
						P <sub>eff</sub> (10 <sup>-6</sup> cm/s)	C <sub>cyto</sub> (mM)	C <sub>mito</sub> (mM)
Alprenolol		9.60 <sup>40</sup>	3.10	3.22	95.70	91.18	7.89	7.82
Atenolol		9.60 <sup>40</sup>	0.16	2.25	1.07	7.44	2.07	5.99
Metoprolol		9.70 <sup>40</sup>	1.88	2.82	40.15	32.28	3.82	8.69
Oxprenolol		9.50 <sup>40</sup>	2.10	2.89	97.25	39.16	4.25	5.76
Pindolol		9.70 <sup>40</sup>	1.75	2.78	54.53	28.78	3.57	8.50
Practolol		9.50 <sup>40</sup>	0.79	2.46	2.91	12.71	2.41	5.03
Propranolol		9.49 <sup>33</sup>	2.98 <sup>31</sup>	3.18	34.80	81.73	7.19	6.03

<sup>a</sup> The log P<sub>n, lip</sub> values were calculated from the published log P<sub>n</sub> values, as described in Methods. References to the Caco-2 data and other relevant measurements are in the Supporting Information.

the delimiting membranes, the mass of drug in each compartment can be modeled using a set of coupled differential equations based on an empirical relationship between lipophilicity and transmembrane permeability of small molecules, and Fick's Law of diffusion.<sup>23</sup> To traverse the cell, molecules first cross the apical membrane, distributing homogeneously in the cytosol and partitioning into cytoplasmic lipids. From the cytosol, they also partition into and out of organelles, and exit the cell across the basolateral membrane.

After simulating the transcellular transport process, the calculated permeability values were found to be consistent with the experimental values. Specifically, we first considered the intracellular concentration and permeability coefficient of molecules with physicochemical properties resembling  $\beta$ -adrenergic receptor blockers: metoprolol and related compounds (Figure 2; Table 1). Metoprolol is orally bioavailable, but less permeable and less toxic than more hydrophobic relatives, such as propranolol.<sup>50</sup> Comparing the calculated results (Table 1) with the experimental data (Table 2), the calculated permeability coefficient of metoprolol is similar to the human permeability coefficient measured in intestinal perfusion experiments,<sup>51</sup> and the coefficient of propranolol is 1 order of magnitude smaller than human permeability coefficients.<sup>51</sup> The *in silico* permeabilities are generally within an order of magnitude of experimentally measured Caco-2 and human intestinal permeability.

**Comparing the Calculated Permeabilities with Experimental Permeability Data.** Correlation of predicted permeability with Caco-2 permeability and human intestinal permeability were plotted to evaluate the model. Figure 2 is the scatter plot of predicted permeability and Caco-2 permeability of seven  $\beta$ -adrenergic receptor blockers—alprenolol, atenolol, metoprolol, oxprenolol, pindolol, practolol, and propranolol—possessing the same core structure (Table 1). This homologous set of drugs has similar pK<sub>a</sub> values (Table 1). A significant relationship was observed.

Next, we examined the correlation of predicted and Caco-2 permeability of 36 structurally unrelated compounds (including the 7 shown in Figure 2; Figure 3). By visual inspection, the predicted permeability of compounds shown in Figure 3 can be readily categorized into two groups: high permeability and low permeability. Using the predicted permeability of metoprolol (No. 18) as a reference (dashed horizontal line), compounds that fall into the dashed oval are predicted to be high permeability by the model and also exhibit high permeability in Caco-2 assays. Most high permeability compounds transport predominantly by the transcellular pathway with some exceptions: for example, P-glycoprotein reportedly affects acebutolol (No. 1 in Figure 3) intestinal absorption.<sup>52</sup> In the scatter plot, the predicted permeability of acebutolol was higher than the Caco-2 permeability, which is consistent with P-glycoprotein efflux not being captured by the model. In contrast, many (predicted) low permeability drugs and molecules possess a significant paracellular or active transport pathway. For example, mannitol (No. 17 in Figure 3) is widely used as a passive paracellular perme-

(49) Palm, K.; Luthman, K.; Ros, J.; Grasjo, J.; Artursson, P. *J. Pharmacol. Exp. Ther.* **1999**, 291 (2), 435–443.

(50) Siebert, G. A.; Hung, D. Y.; Chang, P.; Roberts, M. S. *J. Pharmacol. Exp. Ther.* **2004**, 308 (1), 228–235.

(51) Amidon, G. L. In *The Modern Biopharmaceutics™ Version 6 Computer Based Training Software*; TSRL, Inc: Ann Arbor, MI, 2004.

(52) Terao, T.; Hisanaga, E.; Sai, Y.; Tamai, I.; Tsuji, A. *J. Pharm. Pharmacol.* **1996**, 48 (10), 1083–1089.

**Table 2.** Comparison of Predicted Permeability with Average Caco-2 Permeability and PAMA Permeability of Drugs within the Predictive Oval in Figure 3<sup>a</sup>

drugs	predicted permeability		PAMPA <sup>b</sup>		PAMPA <sup>c</sup> (at pH 7.4)		PAMPA <sup>d</sup> (at pH 7.4)		human intestinal permeability <sup>e</sup>		FDA Waiver Guidance <sup>f</sup>	tentative BCS classification <sup>e</sup>
alprenolol	91.18	H	11.5	H			15.1	H				
antipyrine	209.00	H	2.87	L	0.82	L	13.2	H	560	H	H	
chlorpromazine	653.08	H					4.0	H				1
clonidine	43.82	H	10.41	H			14.0	H				
desipramine	410.18	H	16.98	H			14.6	H	450	H		
diazepam	196.71	H										2
diltiazem	122.32	H	19.21	H	14	H	18.5	H				
ibuprofen	321.84	H	21.15	H			6.8	H				2
imipramine	391.33	H	19.36	H			8.4	H				
indomethacin	406.52	H					2.4	L				
ketoprofen	167.04	H	2.84	L	0.043	L	16.7	H	870	H	H	
lidocaine	126.50	H										
<b>metoprolol</b>	<b>32.28</b>	<b>ref</b>	<b>7.93</b>	<b>ref</b>	<b>1.2</b>	<b>ref</b>	<b>3.5</b>	<b>ref</b>	<b>134</b>	<b>ref</b>	<b>H</b>	
naproxen	175.61	H	5.01	L	0.23	L	10.6	H	850	H	H	
oxprenolol	39.16	H	14.64	H								
phenytoin	86.02	H	38.53	H			5.1	H				
pindolol	28.78	L	4.91	L			4.9	H				
piroxicam	1542.75	H	10.87	H			8.2	H	665	H		
propranolol	81.73	H	26.33	H	12	H	23.5	H	291	H	H	1
trimethoprim	194.22	H	3.14	L	2.2	H	5.0	H				4
valproic acid	144.11	H										3
verapamil	191.16	H	23.02	H	14	H	7.4	H	680	H	H	1
warfarin	129.23	H					12.3	H				

<sup>a</sup> Permeability values are in units of  $10^{-6}$  cm/s. In each published experimental dataset, metoprolol was used as an internal reference compound to define “high permeability” (H) and “low permeability” (L) compounds. <sup>b</sup> Reference 53. <sup>c</sup> Reference 54. <sup>d</sup> Reference 55. <sup>e</sup> Reference 47. <sup>f</sup> Reference 56.

ability marker, so its measured permeability reflects paracellular transport—not only the passive transcellular diffusive permeability that is predicted by the model. Conversely, taurocholic acid and valproic acid are substrates of transporters,<sup>41</sup> which leads to higher measured permeability, well above the passive permeability predicted by the model.

Next, the calculated permeability of compounds that fell into the dashed oval in Figure 3 (those with correctly predicted, high Caco-2 permeability) were compared with PAMPA assay results, as reported in the scientific literature (Table 2). For each individual PAMPA assay result, compounds with higher-than-metoprolol permeability were defined “high permeability” and lower-than-metoprolol permeability were defined “low permeability”.<sup>53–55</sup> Table 2 shows that PAMPA permeability measured in different conditions is different and is affected by buffer conditions.<sup>54</sup> According to FDA waiver guidance<sup>56</sup> the reference drugs ketoprofen and naproxen would be misclassified in two PAMPA measurement, using metoprolol as the internal reference in the published data sets (Table 2). Nevertheless,

both naproxen and ketoprofen are correctly classified by our computational model.

To compare the predicted permeability with human intestinal permeability, a scatter plot was graphed (Figure 4). Since human intestinal permeability data are scarce, among the 36 compounds used in this study (those with experimentally measured log *P*, p*K*<sub>a</sub>, and possessing only one ionizable functional group in the physiological pH range) we only found 10 of them having human intestinal permeability data. A significant linear relationship was obtained.

**Probing the Effect of Drug Physicochemical Properties on Cellular Pharmacokinetics.** The physicochemical properties of drug molecules influence intracellular concentration and transcellular permeability. For a monovalent cationic weak base, the model explicitly considers how three different parameters (the logarithm of the lipid/water partition coefficient of the neutral form of the molecule, log *P*<sub>n</sub>; the logarithm of the lipid/water partition coefficient of the ionized form of the molecule, log *P*<sub>d</sub>; and the negative logarithm of the dissociation constant of the protonated functional group, p*K*<sub>a</sub>) can affect these properties. In silico, one can change

(53) Fujikawa, M.; Ano, R.; Nakao, K.; Shimizu, R.; Akamatsu, M. *Bioorg. Med. Chem.* **2005**, *13* (15), 4721–4732.

(54) Kerns, E. H.; Di, L.; Petusky, S.; Farris, M.; Ley, R.; Jupp, P. J. *Pharm. Sci.* **2004**, *93* (6), 1440–1453.

(55) Zhu, C.; Jiang, L.; Chen, T. M.; Hwang, K. K. *Eur. J. Med. Chem.* **2002**, *37* (5), 399–407.

(56) FDA. *Guidance for Industry: Waiver of In Vivo Bioavailability and Bioequivalence Studies for Immediate-Release Solid Oral Dosage Forms Based on a Biopharmaceutics Classification System*, 2000 ed. <http://www.fda.gov/cder/guidance/3618fnl.pdf> (accessed October 26, 2006).



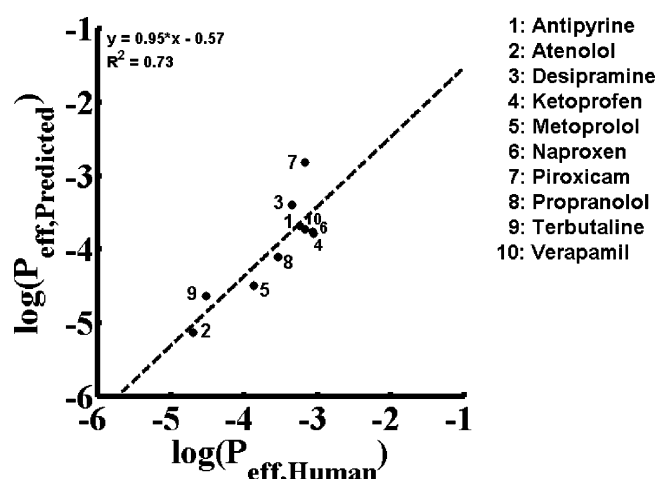


**Figure 4.** Measured human intestinal permeability and predicted permeability are correlated. The x-axis indicates the logarithm values of measured human intestinal permeability (cm/s), and the y-axis indicates the logarithm values of predicted permeability (cm/s), for weakly acidic or basic (nonzwitterionic) drugs with a single ionizable functional group at physiological pH. A simple linear relation was obtained and expressed by the equation  $y = 0.95x - 0.57$  ( $R^2 = 0.73$ ), and the significance  $F$  of regression is 0.0016 (confidence level is 95%). Calculated permeability and human intestinal permeability data is summarized in Table 3.

**Table 3.** Correlation of Predicted Permeability vs Human Intestinal Permeability<sup>a</sup>

name	human permeability <sup>b</sup>	log $P_{\text{eff}}$ , human	predicted permeability	log $P_{\text{eff}}$ , predicted
antipyrine	560.00	-3.25	209.00	-3.68
atenolol	20.00	-4.70	7.44	-5.13
desipramine	450.00	-3.35	410.18	-3.39
ketoprofen	870.00	-3.06	167.04	-3.78
metoprolol	134.00	-3.87	32.28	-4.49
naproxen	850.00	-3.07	175.61	-3.76
piroxicam	665.00	-3.18	1542.75	-2.81
propranolol	291.00	-3.54	81.73	-4.09
terbutaline	30.00 <sup>c</sup>	-4.52	22.96	-4.64
verapamil	680.00	-3.17	191.16	-3.72

<sup>a</sup> Permeability values are in units of  $10^{-6}$  cm/s. <sup>b</sup> Reference 47. <sup>c</sup> Reference 51.

each property one at a time, keeping the others unchanged. Two conditions were considered here: (1)  $\log P_n$  and  $\log P_d$  vary independently (Figure 5A); and (2)  $\log P_n$  and  $\log P_d$  are linked by eqs 27 to 31 (Figure 5B). Although the actual relationship between  $\log P_n$  and  $\log P_d$  of a molecule is neither perfectly linear nor completely independent, simulating these two extremes conditions linking  $\log P_n$  and  $\log P_d$  is one way to assess how physicochemical properties affect calculated permeability and intracellular concentration. For a metoprolol-like molecule cytosolic concentrations remain low and constant as  $\log P_n$  is varied between  $-5$  and  $+3$  (Figure 5A left and Figure 5B left). However, increasing  $\log P_n$  from  $+3$  to  $+5$  increases cytosolic concentration to levels that greatly exceed the extracellular drug concentration. For mitochondrial concentrations, as  $\log$

$P_n$  increases from  $-5$  to  $5$ , there is a pronounced decrease in mitochondrial sequestration. For the transcellular permeability, there is an increase in permeability between  $\log P_n = 3$  and  $\log P_n = 5$ , in parallel to the increase in cytosolic concentration. Thus, for a metoprolol-like molecule, the desired  $\log P_n$  lies between 2 and 3, at which cytosolic and mitochondrial concentrations are minimal, whereas transcellular permeability is maximal.

Just as for the  $\log P_n$  parameter, the  $\log P_d$  values of a metoprolol-like molecule were varied to determine the effect on intracellular concentrations and permeability coefficients. For  $\log P_d$  values less than 2, the intracellular concentration of drug at the steady state is low and constant (Figure 5A middle and Figure 5B middle). However if  $\log P_d$  increases above 2, cytosolic concentrations increase and greatly exceed extracellular drug concentration. For  $\log P_d$  values greater than 3, there is more than a 10-fold increase in mitochondrial concentration above the extracellular concentration. Nevertheless, increasing  $\log P_d$  has the greatest influence on the transcellular permeability value, with increasing  $\log P_d$  associated with the fastest rates of transcellular transport. Thus, according to these simulations, increasing  $\log P_d$  leads to the very desirable effects of increasing transcellular transport rates, although it also leads to the very undesirable effect of increasing cytosolic and mitochondrial drug accumulation.

Finally, the  $pK_a$  value of a metoprolol-like molecule was varied, to study the effect on subcellular transport and biodistribution properties. Compared to the other two parameters, increasing  $pK_a$  from 9 to 14 has little effect on transmembrane permeability (Figure 5A right and Figure 5B right). However, decreasing it from 9 to 7 greatly increased the permeability. Lowering the  $pK_a$  below 9 increased the cytosolic concentration, while increasing it above 9 increased the mitochondrial concentration. Thus the  $pK_a$  of metoprolol is near the point where cytosolic and mitochondrial concentrations are minimized while transcellular permeability is maximized. Again, by varying the physicochemical properties of a metoprolol-like molecule one at a time, the simulations suggests that the cellular pharmacokinetic properties of metoprolol are quite good and would be difficult to improve by varying the physicochemical properties of the molecule, one at a time.

**Chemical Space Definitions and Solutions.** Molecules with intracellular concentrations less than—and permeability values greater than—those for a molecule with metoprolol-like physicochemical properties would possess desirable pharmaceutical features, as these characteristics would be expected to lead to even higher oral bioavailability, improved biodistribution, and decreased metabolism, relative to metoprolol. To identify the physicochemical properties associated with such molecules, we proceeded to calculate the intracellular concentrations and transcellular permeability values of over a million different possible combinations of  $pK_a$ ,  $\log P_n$ , and  $\log P_d$  values. Four different regions of chemical space were defined relative to the steady-state permeability and intracellular concentration of a molecule

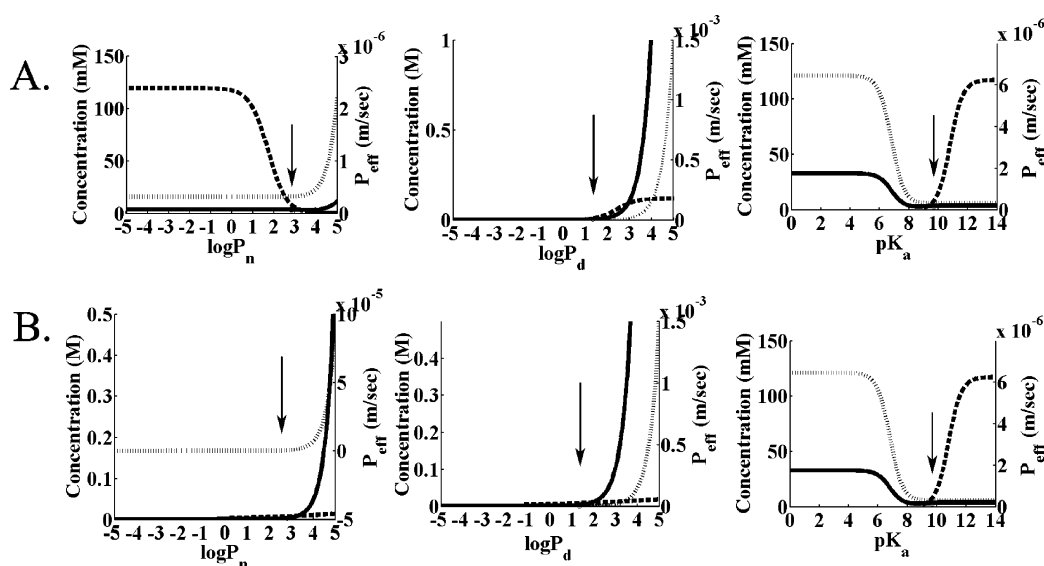


**Figure 5.** Varying one physicochemical property at a time of a molecule with metoprolol-like properties (arrows) affects both the intracellular concentration (solid line = cytosolic; dark dotted line = mitochondrial) and permeability (light stippled line) at steady state. (A) Calculations based on varying  $\log P_n$  and  $\log P_d$  independently from each other. (B) Calculations based on varying  $\log P_n$  and  $\log P_d$  simultaneously, according to the linear relationship expressed as eqs 27–29. Arrows point to the reference liposomal  $\log P_{n, \text{lip}}$ ,  $\log P_{d, \text{lip}}$ , and  $pK_a$  of metoprolol.

with metoprolol-like properties, as follows: (1) Permeant: Molecules with calculated  $P_{\text{eff}}$  equal to or larger than  $P_{\text{eff}}$  of the reference. (2) Impermeant: Molecules with calculated  $P_{\text{eff}}$  less than the reference  $P_{\text{eff}}$ . (3) Nontoxic: Molecules with both  $C_{\text{cyto}}$  and  $C_{\text{mito}}$  equal to or less than  $C_{\text{cyto}}$  and  $C_{\text{mito}}$  of the reference molecule. (4) Toxic: Molecules with either  $C_{\text{cyto}}$  or  $C_{\text{mito}}$  larger than  $C_{\text{cyto}}$  or  $C_{\text{mito}}$  of the reference molecule. Again, two independent set of simulations were carried out, to represent linearly correlated and uncorrelated  $\log P_n$  and  $\log P_d$  values.

Complete analysis of regions of physicochemical property space surrounding molecules with metoprolol-like properties (Figure 6 and Supporting Information) reveal the extent to which cell permeability and intracellular accumulation may be related to the physicochemical properties of the molecules. First, we consider the simulations in which  $\log P_n$  and  $\log P_d$  are varied independently from each other. Note that about 42.7% of total chemical space is occupied by combinations of  $pK_a$ ,  $\log P_n$ , and  $\log P_d$  that would make molecules more permeant than a molecule with metoprolol-like properties (Figure 6A). The remaining 57.3% is occupied by combinations of  $pK_a$ ,  $\log P_n$ , and  $\log P_d$  that would make molecules less permeant than a molecule with metoprolol-like properties. Combinations of  $pK_a$ ,  $\log P_n$ , and  $\log P_d$  that lead to intracellular concentrations greater than those obtained with a molecule with metoprolol-like physicochemical properties lie within “toxic” chemical space, by definition. This region of chemical space comprises 60.6% of the total chemical space, with the remaining 39.4% falling in “nontoxic” space (Figure 6B). If cellular permeability and toxicity were completely unrelated to each other, one would expect that 16.8% of the molecules would fall under “permeant-nontoxic” space (16.8% permeant nontoxic = 39.4% non-

toxic  $\times$  42.7% permeant). However, the actual fraction of molecules falling in cell permeant-nontoxic space (Figure 6C) is 1.5%, as permeability and intracellular accumulation are partly related to each other. Thus, while combinations of  $pK_a$ ,  $\log P_n$ , and  $\log P_d$  promoting permeability and nontoxicity work against each other to some degree, there is a small chunk of physicochemical property space where molecules with greater permeability than metoprolol, but reduced intracellular accumulation, may reside. Indeed, there may be a small but significant number of molecules possessing a desirable combination of physicochemical properties leading to improved bioavailability and biodistribution properties relative to a molecule with metoprolol-like features.

Last, we mapped the chemical space surrounding a molecule with metoprolol-like physicochemical properties, under conditions in which  $\log P_n$  and  $\log P_d$  are perfectly coupled to each other in a linear relationship (Figure 7). Under these conditions, physicochemical property space is reduced to a plane, with a molecule of metoprolol-like features sitting at the intersection of the boundary delimiting permeant–impermeant and toxic–nontoxic space (Figure 7). The impermeant nontoxic and the impermeant toxic were 47.6% and 7.5% of the total space. Most importantly, while permeant toxic occupies 43.7% of the total space respectively, permeant nontoxic occupies 0.11% of this space. Thus, our simulations also indicate that the extent to which  $\log P_n$  and  $\log P_d$  are coupled can severely restrict the ability to find a metoprolol-like molecule with improved biopharmaceutical features. Furthermore, examining where permeant nontoxic space exists relative to metoprolol, one finds that lowering the  $pK_a$  may be the only way to both increase the permeability and decrease the intracellular accumulation

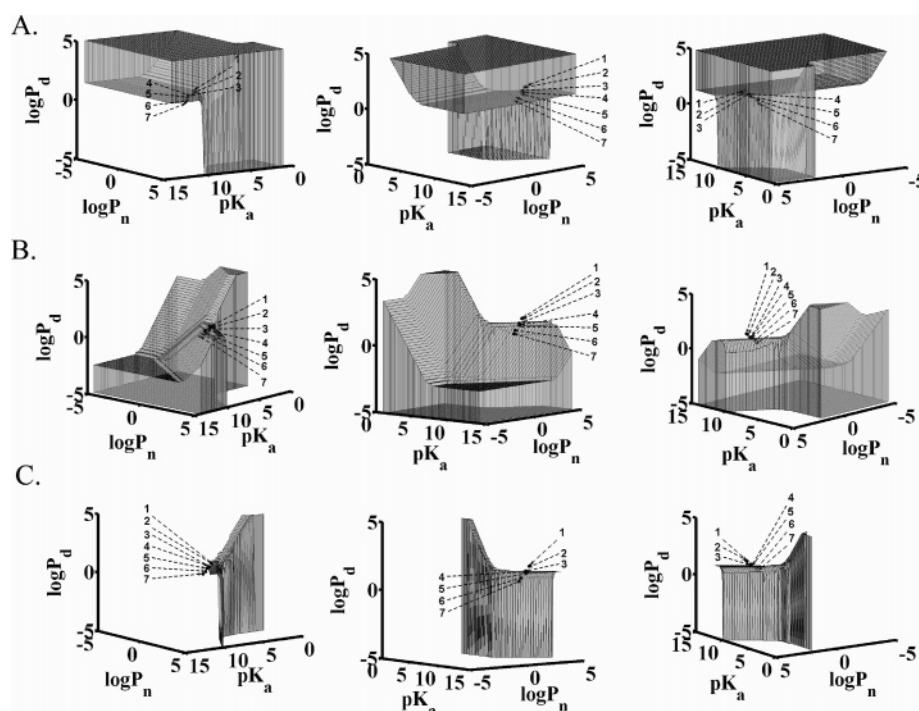


**Figure 6.** The chemical space occupied by molecules with desirable (A) permeability (defined as molecules with calculated  $P_{\text{eff}}$  equal to or larger than  $P_{\text{eff}}$  of a virtual molecule with metoprolol-like properties); (B) intracellular accumulation (defined as molecules with both calculated  $C_{\text{cyto}}$  and  $C_{\text{mito}}$  equal to or less than that of a virtual molecule with metoprolol-like properties); and (C) permeability and intracellular accumulation (defined as molecules with calculated  $P_{\text{eff}}$  equal to or larger than  $P_{\text{eff}}$ , and  $C_{\text{cyto}}$  and  $C_{\text{mito}}$  equal to or less than  $C_{\text{cyto}}$  and  $C_{\text{mito}}$  of a virtual molecule with metoprolol-like properties). Each row is a different (rotated) view of the same, 3D physicochemical property space plot. Calculations of physicochemical property space represent simulations obtained by varying  $\log P_n$  and  $\log P_d$  independently of each other. Numbers 1 through 7 are alprenolol, propranolol, oxprenolol, metoprolol, pindolol, practolol, and atenolol, respectively. The  $\log P_n$  and  $\log P_d$  values of each molecule are the liposomal values, listed in Table 1.

(toxicity) of metoprolol. For the  $\beta$ -blockers, the  $pK_a$  of the molecule is determined by an isopropyl amine group that is shared by all the congeners (Table 1), and therefore this group may be essential for receptor binding. One way around this constraint would be to change the ionization properties of the molecules by making them zwitterionic at physiological pH. However, the current model cannot capture the behavior of zwitterions, so a theoretical analysis of this optimization strategy must await development and validation of more advanced versions of the model.

## Discussion

Transport of small molecules into and out of cells and organelles is determined by both passive and active transport mechanisms. The cellular pharmacokinetic model elaborated in this study specifically captures passive transport mechanisms, determined by the physicochemical properties of small molecules, their interactions with phospholipid bilayers, and the concentration gradients of ions and macromolecules across cellular membranes.<sup>22,48,57,58</sup> Empirical<sup>12,22,59</sup> and

theoretical<sup>60–62</sup> considerations establish three physicochemical properties of small molecules as key determinants of passive transport across membranes: size, charge, and lipophilicity. Most molecules used for drug discovery and chemical genomics investigations are “small”, i.e. between 200 and 800 daltons, and therefore similar in size. Thus, the model is suitable for comparing the behavior of small molecules within this limited size range, where the main physicochemical properties influencing the distribution of molecules in cells are the multiple ionization states, and the lipophilicity of each ion.

For model validation, metoprolol was used as a reference because it is an FDA-approved drug that is 95% absorbed in the gastrointestinal tract,<sup>1</sup> and it is recommended as an internal standard—to be included in experiments that assess drug permeability<sup>56</sup>—by the FDA. Metoprolol is generally included in published PAMPA, Caco-2, and intestinal

(57) Artursson, P.; Palm, K.; Luthman, K. *Adv. Drug Delivery Rev.* **2001**, *46* (1–3), 27–43.

(58) Malkia, A.; Murtomaki, L.; Urtti, A.; Kontturi, K. *Eur. J. Pharm. Sci.* **2004**, *23* (1), 13–47.

(59) Lipinski, C. A.; Lombardo, F.; Dominy, B. W.; Feeney, P. J. *Adv. Drug Delivery Rev.* **2001**, *46* (1–3), 3–26.

(60) Flewelling, R. F.; Hubbell, W. L. *Biophys. J.* **1986**, *49* (2), 541–552.

(61) Flewelling, R. F.; Hubbell, W. L. *Biophys. J.* **1986**, *49* (2), 531–540.

(62) Schamberger, J.; Clarke, R. J. *Biophys. J.* **2002**, *82* (6), 3081–3088.



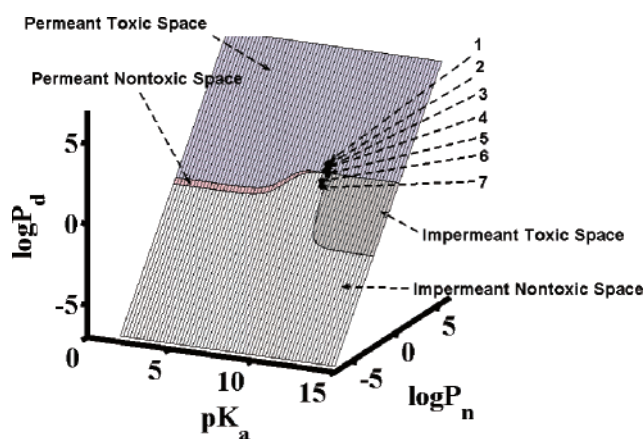


**Figure 7.** The calculated physicochemical property space occupied by molecules with permeant, impermeant, toxic, and nontoxic molecules, relative to a metoprolol-like reference molecule. Calculations represent results obtained by varying  $\log P_n$  and  $\log P_d$  simultaneously, according to the simple linear relationship expressed in eqs 27–29. Numbers 1 through 7 are alprenolol, propranolol, oxprenolol, metoprolol, pindolol, practolol, and atenolol, respectively. The  $\log P_n$  and  $\log P_d$  values of each molecule are liposomal values, listed in Table 1.

permeability datasets, as a reference point with which to establish the threshold between high and low permeability compounds. Several metoprolol relatives—like atenolol—are orally bioavailable, moderate absorption, low metabolism, low toxicity, renally cleared<sup>36,63–66</sup> with a well-characterized, passive-transport absorption mechanism,<sup>67</sup> in vitro and in vivo permeability characteristics,<sup>51,68</sup> and measured micro  $pK_a/(\log P)$  properties.<sup>34</sup> Using the physicochemical properties of metoprolol as a reference, cell-based molecular transport simulations were used to calculate the pharmaceutical properties of related  $\beta$ -adrenergic receptor antagonists. Setting cellular parameters and model geometry to mimic an intestinal epithelial cell, the simulations permitted testing the effects of different biological and chemical parameters on intracellular concentrations and transcellular permeability coefficients, through time. The steady-state values for high permeability compounds were comparable to experimental measurements obtained through intestinal, in vivo perfusion experiments, and Caco-2, in vitro permeability assays.<sup>22,69,70</sup> In addition, running over a million different combinations

of  $\log P_n$ ,  $\log P_d$ , and  $pK_a$  through the simulation allowed us to define a physicochemical property space leading to the most desirable biopharmaceutical characteristic (higher transcellular permeability with lower intracellular accumulation), relative to the simulated characteristics of a metoprolol-like molecule.

We note that, since intracellular accumulation and permeability are related to each other, optimizing a single biopharmaceutical property (permeability) of a compound at a time may lead to unfavorable biodistribution properties (intracellular accumulation) associated with toxicity or drug clearance by metabolism. Indeed, complex properties like bioavailability may be predictable as nonlinear functions of the fundamental physicochemical properties of molecules, under conditions in which transcellular transport is maximized and intracellular concentrations are minimized. Due to the limited experimental data available for fitting statistical models, and the relatively complex behaviors apparent in the simplified model presented in this study, our results suggest that purely empirical, statistical regression models built from human, Caco-2, or even PAMPA permeability data would be comparatively limited in their ability to predict bioavailability of small molecule drugs. Thus, cellular pharmacokinetic simulations could be used to complement to the more conventional, regression-based statistical approaches. This is especially true in situations when the statistical models lack power, such as when assay measurements are too variable or of low quality, or when a training dataset is unavailable, of dubious quality, or too sparse. With continued validation and refinement, cell-based mass transport simulators can become increasingly sophisticated in their ability to capture more complex phenomena of pharmaceutical importance.

Admittedly the scope of the current, passive diffusion model is narrow, as its predictions apply only to nonzwitterionic, monocharged molecules within a limited size range, administered at high concentrations so that they saturate specific binding sites on intracellular proteins, enzymes, and transporters. However the therapeutic impact of the model could be substantial, since 80% of currently marketed therapeutic products are small molecules, administered orally and at high concentrations.<sup>19</sup> Moreover the majority of these do target cell surface receptors or ion channels.<sup>9</sup> The FDA's Biopharmaceutics Classification System<sup>47</sup> recognizes four classes of oral drug products: class I (high solubility–high permeability); class II (low solubility–high permeability); class III (high solubility–low permeability); and class IV (low solubility–low permeability). The model is mostly relevant to class I and II small molecule drugs, which turn out to be very common and well-behaved, encompassing about half of the drug products on the market.<sup>19</sup> Since extracellular receptor binding allows maximizing a drug's transcellular permeability while minimizing intracellular accumulation, our model provides a mechanistic explanation

- (63) Borchard, U. *Clin. Physiol. Biochem.* **1990**, 8 (Suppl. 2), 28–34.
- (64) Kirch, W.; Gorg, K. G. *Eur J. Drug Metab. Pharmacokinet.* **1982**, 7 (2), 81–91.
- (65) Mehvar, R.; Gross, M. E.; Kreamer, R. N. *J. Pharm. Sci.* **1990**, 79 (10), 881–885.
- (66) Riddell, J. G.; Harron, D. W.; Shanks, R. G. *Clin. Pharmacokinet.* **1987**, 12 (5), 305–320.
- (67) Neuhoff, S.; Ungell, A. L.; Zamora, I.; Artursson, P. *Pharm. Res.* **2003**, 20 (8), 1141–1148.
- (68) Walter, E.; Janich, S.; Roessler, B. J.; Hilfinger, J. M.; Amidon, G. L. *J. Pharm. Sci.* **1996**, 85 (10), 1070–1076.
- (69) Egan, W. J.; Lauri, G. *Adv. Drug Delivery Rev.* **2002**, 54 (3), 273–289.

- (70) Kulkarni, A.; Han, Y.; Hopfinger, A. J. *J. Chem. Inf. Comput. Sci.* **2002**, 42 (2), 331–342.



as to why the major class of well-behaved, orally bioavailable drugs currently on the market does often target extracellular domains of cell surface receptors.

To conclude, cell-based molecular transport simulators can be used to make other predictions in addition to transcellular permeability, which could also be experimentally tested. Because each component that goes into the model can be studied and improved independently, more precise membrane transport equations including additional variables (such as molecular weight)<sup>60,62</sup> and additional subcellular compartments could be readily incorporated into the models, albeit at the expense of greater computational complexity. Indeed, by checking predictions with experiments, the model can be gradually improved and evolved, and its scope can be extended to describe the transport of an increasing variety of molecules (such as zwitterions), under increasingly diverse conditions. Using single cells as pharmacokinetic units, it should be possible to model transport functions in multicellular organizations, simulating transport functions in tissues and even organs, and even incorporate intracellular enzymatic, transporter, and specific binding and nonspecific absorption activities through the Michaelis–Menten equation and binding isotherms. By coupling cell-based, molecular transport simulators to other cheminformatic analysis tools (such as computational  $pK_a$  and log  $P$  calculators), *in silico*

screening experiments may be performed—rapidly, inexpensively, reproducibly, and reliably—on a large number of molecules, to explore the diversity of large collections of molecules in terms of their cellular pharmacokinetic and pharmacodynamic properties.

**Acknowledgment.** This work was supported by NIH Grant HG003890. X.Z. expresses thanks for the support from the Fred Lyons Jr. Fellowship and the Schering-Plough Graduate Fellowship from the College of Pharmacy at The University of Michigan. Many thanks to Drs. Stefan Trapp and Richard W. Horobin for help with the original model<sup>23</sup> as well as critical reading of the manuscript. Thanks also to L. Benet, G. Drusano, P. G. Schultz, G. Crippen, T. Oprea, G. Cruciani, G. L. Amidon, and anonymous reviewers, for insights, suggestions, discussions, and encouragement.

**Supporting Information Available:** The parameters used in the calculations, exploration of the effects of cellular variables on steady-state permeability and concentrations, additional validation of the model and chemical space maps under a variety of different conditions, and the MATLAB solvers and graphing scripts. This material is available free of charge via the Internet at <http://pubs.acs.org>.

MP060046K